Eur. Phys. J. E (2015) **38**: 26
DOI 10.1140/epje/i2015-15026-3

THE EUROPEAN PHYSICAL JOURNAL E

Regular Article

Contribution to the benchmark for ternary mixtures: Measurement of diffusion and Soret coefficients of ternary system tetrahydronaphtalene–isobutylbenzene–n-dodecane with mass fractions 80-10-10 at 25 °C*

Quentin Galand[a] and Stéfan Van Vaerenbergh

Microgravity Research Center, Université libre de Bruxelles, Dept. Chemical Physics, Avenue F. D. Roosevelt, CP165/32, B-1050, Brussels, Belgium

Received 16 July 2014 and Received in final form 19 November 2014
Published online: 27 April 2015 –

Abstract. This paper provides the molecular diffusion and Soret coefficients of the ternary system 1,2,3,4-tetrahydronaphtalene, isobutylbenzene, *n*-dodecane system at mass fractions 0.8-0.1-0.1 and temperature 25 °C for implementation into the benchmark presented in this topical issue. The Soret coefficients are determined by digital interferometry using the data of DSC-DCMIX microgravity experiment. The method used takes into account the influence of the thermal field on the Soret separations and the selection of the image processing techniques results in reproducible Soret coefficients.The diffusion coefficients are obtained by the Open Ended Capillary technique The fitting of the data collected through a set of two complementary experimental runs allows retrieving the four Fickian diffusion coefficients.

1 Introduction

Interest on the topic of diffusion properties of ternary liquid systems motivated several research teams to perform benchmark measurements of the molecular diffusion and Soret coefficients of the ternary system composed of tetrahydronaphtalene (THN), isobutylbenzene (IBB) and *n*-dodecane (*n*C12) with respective mass fractions 0.8-0.1-0.1 and at 25 °C using different experimental techniques [1]. This paper is our contribution to this benchmark and summarizes the results obtained from two different experiments: the Soret coefficients were obtained under reduced-gravity conditions on the International Space Station (ISS) by a digital interferometric technique during the DSC-DCMIX1 (Diffusion and Soret Coefficients —Diffusion Coefficients in Mixtures) experiment and the molecular diffusion coefficients were measured by the Open Ended Capillary technique (OEC).

The DSC-DCMIX1 experiment was performed in reduced-gravity conditions inside the European Space Agency SODI multi-user facility (Selectable Optical Diagnostics Instrument) aboard the ISS. The SODI multipurpose facility allowed conducting several experiments: DSC, IVIDIL [2], COLLOID and DSC-DCMIX1 (2011-2012) and is hosted on the International Space Station. In DSC-DCMIX1 a cell array of six cells, one containing a binary mixture, and five containing ternary mixtures at different compositions, was installed in the interferometric, two wavelengths optical set-up of SODI. The purpose of this experiment is to acquire on board the data allowing the determination of the Soret and diffusion coefficients in the ternary liquid mixtures at mean temperatures of 25 °C and 40 °C. The experimental conditions are such that species transport results from thermal gradient and molecular diffusion. In a ternary system, the diffusive flux J_i of component i can be written as [3,4]

$$J_i = -\rho \sum_{j=1}^{2} D_{ij} \nabla w_j - \rho D'_{T,i} \nabla T, \tag{1}$$

where ρ is the density of the liquid, D_{ij} are the molecular diffusion coefficients, w_i and $D_{T,i}$ are, respectively, the mass fraction and the thermodiffusion coefficients of component i, and T is the temperature. Once the system has reached a steady state in a closed cell, with no convection and no chemical reactions, the diffusion fluxes vanish and the composition along the cell is proportional to the temperature gradient. From eq. (1) this can be written as

$$\nabla w_i = -S'_{T,i} \nabla T, \tag{2}$$

where we introduced the modified Soret coefficients $S'_{T,i}$. Although this steady state is reached only after an infinite time, 99% of the separation is obtained after about

* Contribution to the Topical Issue "Thermal non-equilibrium phenomena in multi-component fluids" edited by Fabrizio Croccolo and Henri Bataller.

[a] e-mail: qgaland@ulb.ac.be

five times the species diffusion relaxation time. This corresponds in on-board operations to the end of the "Soret phase". It must be *a posteriori* verified that the process is close to completion.

The so-obtained concentration differences Δw_i of the components across the cell provide the Soret coefficients by the relation

$$\Delta w_i = -S'_{T,i}\Delta T, \tag{3}$$

where ΔT is the temperature difference from the top to the bottom walls of the cell. After the "Soret phase", the temperature gradient imposed at the boundaries is suppressed; the "diffusion phase" then develops and eq. (1) applies with a vanishing temperature gradient

$$J_i = -\rho \sum_{j=1}^{2} D_{ij} \nabla w_j. \tag{4}$$

The succession of these two phases allows retrieving the set of all independent Soret coefficients and molecular diffusion coefficients for each of the cells studied. The DSC-DCMIX1 experiment delivered the large amount of thermal and interferometric data needed to retrieve all the coefficients. In this paper, we report part of this work by providing the Soret coefficients for the benchmark system [1], for three distincts experimental runs, referred to as runs 3, 18 and 23. We first briefly provide in sect. 2.1 the experimental details and image processing method needed for this analysis. In sect. 3.1, we discuss the results under the perspective of the thermics and image processing and provide the Soret coefficients.

OEC is a well-known technique for the measurement of isothermal diffusion coefficients. This technique is used to study isothermal diffusion (eq. (4)). It was first used in 1949 to study self-diffusion in liquids with the help of isotopic tracers [5]. Since then, the technique has been adapted to the study of mutual diffusion in binary systems, consisting of electrolytes [6], gases [7], and organic liquids [8]. It was extended to the study of multicomponent liquid system by Leahy-Dios *et al.* [9]. They reported the diffusion coefficients of the liquid system composed of *n*-octane, *n*-decane and 1-methylnaphtalene, and they obtained the concentration of the samples by coupling density and refractive index measurements. These results have inspired us and led us to develop an Open Ended Capillary set-up that was studied in details in [10], where we obtain very accurate measurements of the concentration of the samples by nuclear magnetic resonance measurements. In addition, for the first time in the present paper, we introduce a significant improvement of the experimental procedure: for the measurement of the molecular diffusion in one single system, we perform two completely independent experiments, as suggested in [11] For each of these, the gradients of the chemical concentration of the three components are very different. The experimental data collected through both experiments are combined to perform the calculation of the entire matrix of the diffusion coefficients, as detailed in sect. 3.2.

2 Material and methods

2.1 Measurement of Soret coefficients

2.1.1 DSC-DCMIX1 set-up and timeline

The SODI facility and the DSC-DCMIX1 set-up were described in details in *e.g.* refs. [2,4]. The liquid is contained in a transparent square quartz frame that is clamped between two machined copper parts (the "heat blocks" in fig. 1), one of which contains a small volume expansion compensation chamber. The thickness of liquid (x and y directions) is $e = 10\,\text{mm}$ and the internal height (z direction) of the cell is $L = 5\,\text{mm}$. The temperature of each heat block is probed with calibrated thermal sensors for a temperature reading with a resolution of 0.01 K. The temperature control is implemented through Peltier elements and the cell is enclosed in a case of insulating material to limit lateral heat losses and insulate from the fan's air flow.

Prior to a run, the temperature of the top heat block, T_1, and the one of the bottom heat block, T_2, are stabilized at 25 °C during two hours. Then, the run goes as follows: a temperature difference of 10 °C is applied across the cell during the "Soret phase": T_1 and T_2 are, respectively, set to 30 °C and 20 °C. The resulting thermal field in the liquid induces the migration of the chemical components by thermodiffusive process. Then, in the second phase, the "diffusion phase", the heat blocks temperature difference is removed and the composition evolves towards homogeneous state by molecular diffusion. For runs 18 and 23 (respectively 3), the "Soret phase" lasted about 6 hours (respectively 9 hours) while the duration of the "diffusion phase" was 4 hours (respectively 6 hours).

2.1.2 Optical signals

A two-wavelengths Mach-Zehnder set-up of SODI provides interferograms recorded at a suitable rate. The coherent light sources are a $\lambda_1 = 670\,\text{nm}$ (red) and a $\lambda_2 = 935\,\text{nm}$ (near infrared) laser diode. Phase shifting interferometry [12] was used and phase shifts obtained by stepping the laser diode currents. The selected technique is based on the acquisition of a set of five fringe images acquired in less than a second for both wavelengths

The temperature and composition fields variations in the liquid are obtained by analyzing the changes of the refractive indexes n_i fields at the two different wavelengths λ_i, as described in sects. 3.1.2 and 3.1.3. Experimentaly, the variation $\mathrm{d}n_i$ of refractive index at wavelength i is obtained from the corresponding phase difference $\mathrm{d}\varphi_i$ that is recorded on interferograms

$$\mathrm{d}n_i = \frac{\lambda_i}{2\pi e}\mathrm{d}\varphi_i. \tag{5}$$

The image post-processing procedure implemented to translate the experimental images to the phase changes maps includes several steps. First, phase signals of each

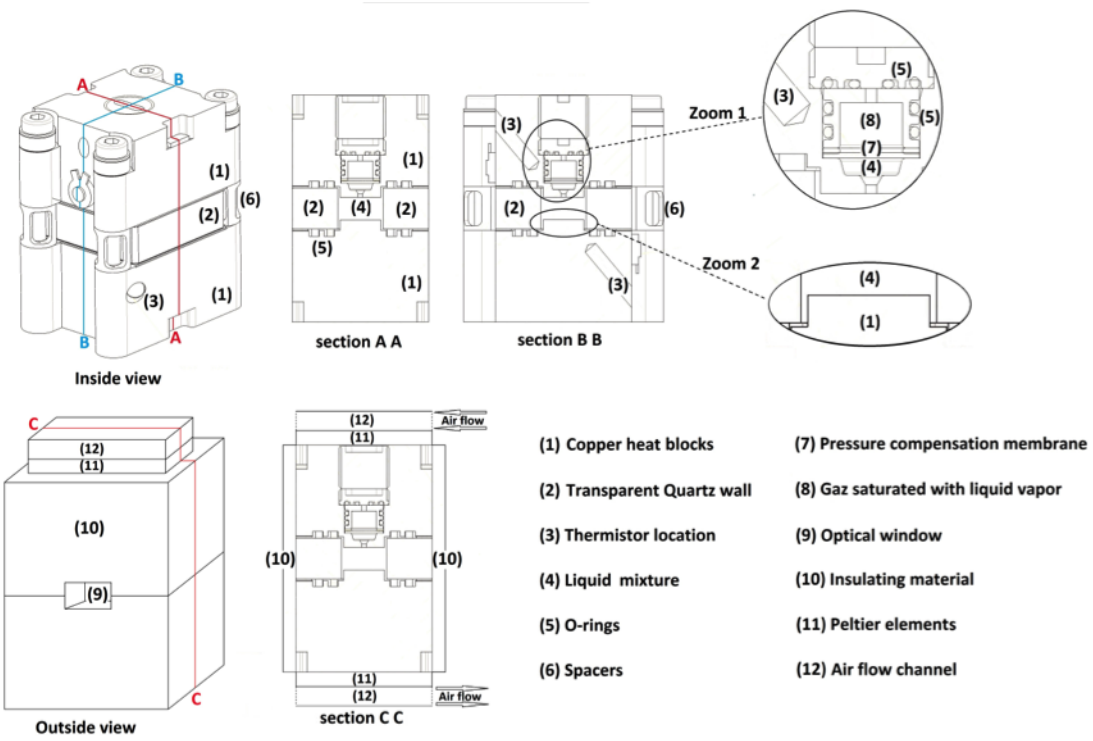

Fig. 1. Schematic of a DCMIX experimental cell.

acquired interference patterns are computed. Different image processing algorithm can be used, such as the Fourier transform technique [13,14] or phase-shifting methods [12, 15]. Here, we used phase-shifting. Due to important variations of the amplitude observed for the phase shifts, the method was adapted using an iterative algorithm, as described in [16]. In the second step of image post processing, a reference image is subtracted. Depending on the choice of the reference image, several contributions in the phase variation signals can be discriminated [17]. In this work, the reference image for each wavelength is chosen when the temperature and the concentration of the liquid are homogeneous across the cell. This experimental image used was acquired at the end of the thermal stabilization phase of the experiment, prior to the start of the "Soret phase". Then, in the third step, the phase signal, that is modulo 2π, must be unwrapped to construct a natural phase. Due to the noisy signals resulting from the performances of SODI and from the phase shifting calculations, the simplest phase unwrapping approach, as the successive comparison of closed neighbor pixels [18] or Fourier method unwrapping [19] did not provide accurate results. Instead, we performed accurate unwrapping by a Costantini algorithm, described in [20].

2.2 Measurement of diffusion coefficients

In an OEC experimental run, two solutions of different compositions are placed in contact as follows: at the beginning of the experiment, several "capillary" tubes, with an open end, are filled with a solution of composition w_0 and are immersed in a bath maintained at constant composition w_∞, as shown in fig. 2.

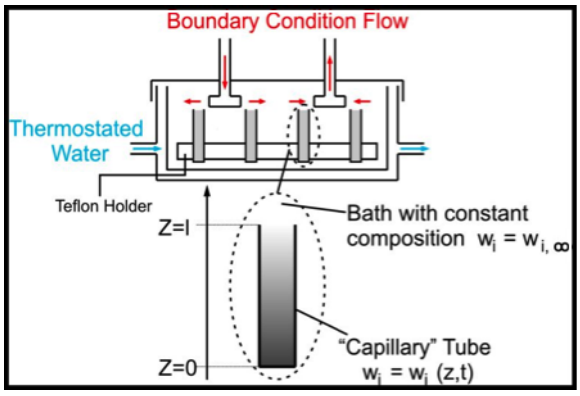

Fig. 2. Schematic of our experimental set up for the OEC technique.

Measurement of accurate diffusion coefficients requires avoiding parasitic convective mass transfer. In order to maintain the liquid in a stable configuration from the hydrodynamic point of view, the initial solution inside the capillary tubes is more concentrated in the heavier component and is thus denser than the solution of the bath.The accurate mathematical description of the diffusive process also requires maintaining a constant composition at the outlet of the capillaries. The liquid of the bath is continuously refreshed by flowing liquid from a higher tank, trough the cell and towards a lower tank (see fig. 2). The tanks are regularly reversed so that the flow is continuous. Inside the tubes, a diffusive profile of the chemical composition develops over time and results in an evolution of the average composition. Experimentally, capillaries are regularly extracted from the bath and their composition

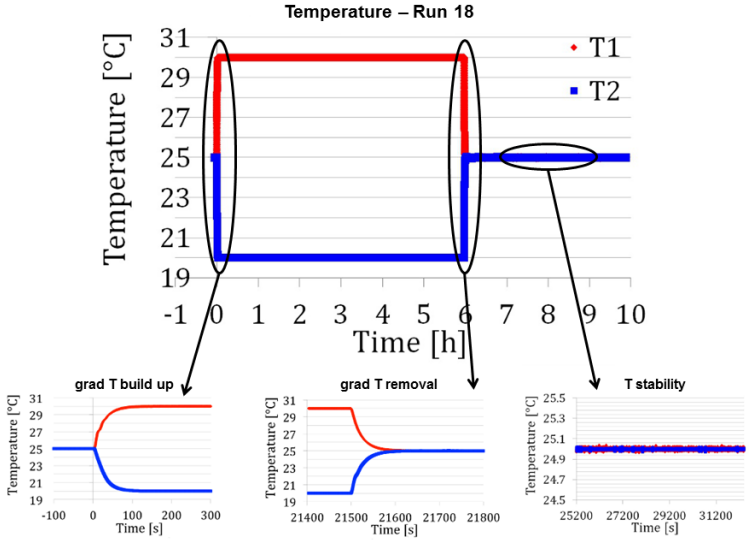

Fig. 3. Typical temperature cycle performed in a DSC-DCMIX1 run on cell 3 at 25 °C. In the bottom of the figure, several zooms are showed to illustrate the performances of the temperature regulation.

is quantified. The entire matrix of diffusion coefficients is estimated by fitting the temporal evolution of the composition, as detailed in sect. 3.2. Composition analysis of the samples was obtained by proton NMR, using the experimental protocol described in details in [10]. The absolute errors on the mass fractions measurement with this technique were estimated using samples of known composition and found to be lower than ±0.001. Mathematical description of the OEC technique was detailed in [10]. The measuring cell is cylindrical, with height about 10 cm, and internal diameter 10 cm. The internal height of the tubes is about 4.5 cm and was calibrated for each tube, with a precision of $l \pm 10^{-4}$ m, that is to say of the order of 0.2%. The internal diameter of the tubes is 1 mm. The glass container is double jacked for thermostated water (±0.1 K) circulation and sealed by a TEFLON® O-ring to avoid evaporation.

3 Results and discussion

3.1 Measurement of Soret coefficients

3.1.1 Thermal regulation

Figure 3 shows the evolution of the temperatures T_1 and T_2, respectively, of the top and bottom copper blocks of cell 3 measured during one of the DSC-DCMIX1 experimental runs (run 18). Similar results were observed for other runs investigated (runs 3 and 23).

Details of the regulation while applying (respectively removing) the temperature difference at the beginning of the "diffusion phase" (respectively "Soret phase") are shown in the two first zooms at the bottom of fig. 3. For all the runs 90% of the temperature difference is established or removed within a little less than 1 minute, and 99% is reached within 2 minutes. The third zoom shows that the temperature regulation is stable and precise: during the "Soret phase", the maximum deviation between the measured and set point temperatures is 0.02 °C; during the "diffusion phase", it is 0.05 °C.

3.1.2 Temperature field across the cell

The temperature field in the liquid can be obtained from the interferometric measurements. The data is obtained for cell 0 filled with a binary mixture of THN and nC12, with equal mass fractions. The temperature field is computed by subtracting a reference image acquired during the thermal stabilization phase of the runs (*i.e.* when $T_1 = T_2 = 25\,°\mathrm{C}$) to the image acquired approximately two minutes (*i.e.* more than 5 times the characteristic heat diffusion time of the liquid) after the stabilization of the temperature control. The corresponding phase images were calculated and processed as described in sect. 2.1.2. The phase change $\mathrm{d}\varphi$ was corrected to remove the contribution of the refractive index change in the cell's glass, as discussed in [17], by assuming a linear distribution of the temperature along the z direction in the glass. The refractive index change $\mathrm{d}n$ is calculated with eq. (5) and translated to the temperature difference

$$\mathrm{d}T = \mathrm{d}n \left(\frac{\partial n}{\partial T} \right)^{-1}, \tag{6}$$

with the following values for the calculations: temperature contrast factor of the liquid $(\partial n/\partial T)_{\mathrm{liquid}} = -4.39 \cdot 10^{-4}$ [21], geometric path in the liquid $e_{\mathrm{liquid}} = 10\,\mathrm{mm}$, temperature contrast factor of the glass $(\partial n/\partial T)_{\mathrm{glass}} = 10^{-5}$, geometric path in the glass $e_{\mathrm{glass}} = 20\,\mathrm{mm}$.

The obtained temperature field is shown in fig. 4. It is seen that the design of the cell and the lateral heat losses induce a strong curvature of the temperature field

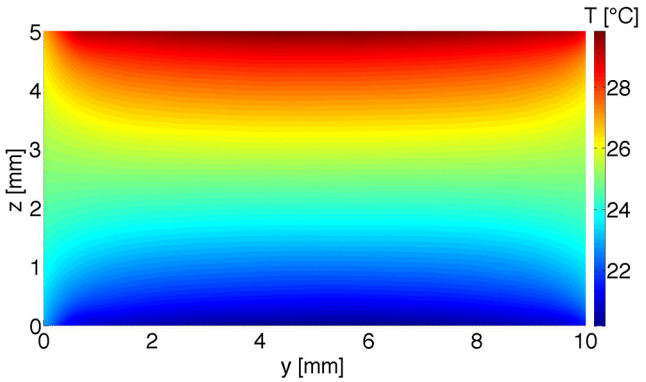

Fig. 4. Colormap of the temperature observed cell 0 during a run at 25 °C of the DSC-DCMIX1 experiment.

approaching the lateral edges of the cell. The temperature difference between the top and bottom of the cell is close to 10 °C at the center of the cell; in the case of the run plotted in fig. 4, we calculated a temperature difference of 9.89 °C. The temperature difference is significantly reduced when approaching the lateral walls of the cell, respectively of about 5%, 8% and 11% along vertical located at 2 mm, 1.5 mm and 1 mm of the glass wall. It must be emphasized that the optical signals are influenced also by several parameters such as the choice of the reference image, the stability of the optics, the algorithms used for the image processing and the temperature fluctuations in the liquid, so that the values obtained for different runs are not exactly the same. Here we use the value of the temperature difference of 10 °C for the Soret coefficients determination. However, to limit the influence of the deformation of the temperature field, only the central region of the field of view of the experimental images, including 70 percent of the pixels along the horizontal axis y are used for the fittings. This region of interest is also limited in the z direction, as explained in the next paragraph.

3.1.3 Evaluation of the Soret coefficients

In this work we determine the Soret coefficients by a procedure that does not use molecular diffusion coefficients to avoid the multiplication of uncertainty sources. The Soret separations are evaluated by subtracting a reference image, corresponding to the isothermal and homogeneous liquid system and taken at the end of the thermal stabilization of the runs, to an image containing the Soret concentration separations of the component. The later image is acquired at a time t_0 after the end of the "Soret phase" larger than the duration of the temperature transients resulting from the removal of the temperature difference at the copper heat blocks. This time is typically five times the thermal characteristic time, and still much smaller than the species diffusion characteristic times. During this time molecular diffusion starts and creates concentration changes limited to the regions close to the top and bottom walls of the cell, as discussed in [22]. This effect does not need to be taken into account in our procedure if we limit

Table 1. Contrast factors for the system THN-IBB-nC12 studied in cell 3 of the DSC-DCMIX1 experiment at $T = 25\,°C$. Component 1 is 1,2,3,4-tetrahydronaphtalene, component 2 is isobutylbenzene and component 3 is n-dodecane. Those values were computed from [4].

Cell	w_1	w_2	w_3	$n_{1,1}\|_2$	$n_{1,2}\|_1$	$n_{2,1}\|_2$	$n_{2,2}\|_1$
3	80	10	10	0.142775	0.088696	0.137367	0.083769

the analysis of the experimental data to central 90 percent of the field of view along a vertical of the cell.

To test the validity of the used region of interest, the experimental phase images $\mathrm{d}\varphi_i$ for both wavelengths are calculated and processed on the full field of view. Results are shown in fig. 5. On it, the approximated linear fitting function $\mathrm{d}\varphi_{i,\mathrm{fit}}$ is also shown. The fitting error ε_i defined as

$$\varepsilon_i = \mathrm{d}\varphi_i - \mathrm{d}\varphi_{i,\mathrm{fit}} \tag{7}$$

can be made very small by a good selection of the region of interest, and in particular by the one defined above (centered, 70% in lateral direction and 90% along the gradient).

The phase differences from the top to the bottom of the cell $\Delta\varphi_i$ are calculated by extrapolating the fitting function $\mathrm{d}\varphi_{i,\mathrm{fit}}$ to the entire height of the cell

$$\Delta\varphi_i = \mathrm{d}\varphi_{i,\mathrm{fit}}(z = L) - \mathrm{d}\varphi_{i,\mathrm{fit}}(z = 0). \tag{8}$$

The precision of the linear fitting in determining the $\Delta\varphi_i$ can be quantified by the standard deviations $\sigma_{\Delta\varphi_i}$ reported in table 2. These are calculated for each individual fitting by quantifying the dispersion of the experimental data points from the fitting planes.

The refractive index differences Δn_i are computed with eq. (5) and converted to the Soret separations with

$$\begin{pmatrix} \Delta w_1 \\ \Delta w_2 \end{pmatrix} = \begin{pmatrix} n_{1,1}\|_2 & n_{1,2}\|_1 \\ n_{2,1}\|_2 & n_{2,2}\|_1 \end{pmatrix}^{-1} \begin{pmatrix} \Delta n_1 \\ \Delta n_2 \end{pmatrix}. \tag{9}$$

In eq. (9) we introduced the matrix of the concentration contrast factors whose coefficients $n_{i,j}|_k$ are defined by

$$n_{i,j}\big|_k = \left.\frac{\partial n_i}{\partial w_j}\right|_{T,P,w_k,k\neq j}. \tag{10}$$

The computed values of the Soret coefficients strongly depend on the values of the contrast factors used for the calculations. The contrast factor matrix is obtained using the methodology and the experimental data reported in [23]. The values of the $n_{i,j}|_k$ used here are reported in table 1. Finally, the coefficients $S'_{T,i}$ are deduced from eq. (3). The errors on the obtained Soret coefficients $\Delta S'_{T,i}$ are evaluated by calculating the propagation of the relative errors on the $\Delta\varphi_i$, on the contrast factors and on the temperature measurements, through eqs. (3), (5) and (9). In these calculations, we used relative errors on the $\Delta\varphi_i$ inferred from the absolute average deviation of the contrast factors of 2.4% reported in [23] and maximal error

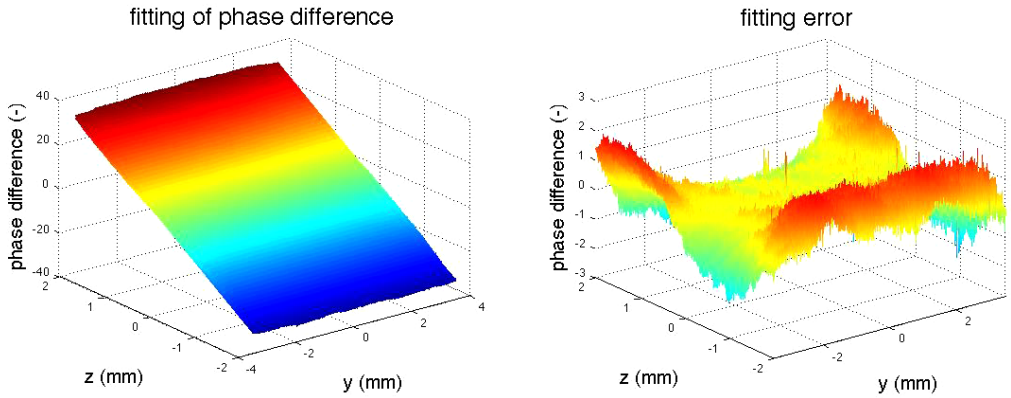

Fig. 5. Typical linear fitting to obtain the Soret separation at the end of the "Soret phase". Data obtained for cell 3, run 3 and wavelength $\lambda_2 = 935\,\text{nm}$. Left: comparison of the experimental signal to the linear fitting. Right: fitting error, defined as the difference between the experimental signal and the fitting function.

Table 2. Phase differences with corresponding standard deviations and refractive index differences from the top to the bottom of the cells at the end of the "*diffusion phase*" for DSC-DCMIX1 runs 3, 18 and 23 at $T = 25\,^{\circ}\text{C}$.

Cell	Run	$\Delta\varphi_1$	$\sigma_{\Delta\varphi_1}$	$\Delta\varphi_2$	$\sigma_{\Delta\varphi_2}$	$\Delta n_1\,10^3$	$\Delta n_2\,10^3$
3	3	111.8	0.8	78.0	0.5	1.192	1.160
	18	111.6	1.1	77.8	0.9	1.189	1.158
	23	106.2	0.9	77.6	0.6	1.184	1.155

of 0.1 K on thermistors readings for the measurements of temperatures T_1 and T_2. In doing so, we obtain the maximal errors $\Delta S'_{T,i}$ on the estimated Soret coefficients.

The obtained phase and refractive index differences are reported in table 2 and the Soret separations and coefficients are reported in table 3.

3.1.4 Discussion of results

There exist several procedures to retrieve the Soret coefficients from digital interferometry experiment. One approach, used in [17] for binary systems, consists in solving the diffusion equation and fitting the experimental data to obtain simultaneously the diffusion and Soret coefficients. In binary systems, this analysis implies a fitting involving two unknowns, one diffusion and one Soret coefficients. In [17], the authors introduce a third fitting variable, an initial time t_0, which allow taking into account the thermodiffusive separation of the components during the thermal transients. Applying a similar procedure to ternary systems means fitting simultaneously 4 unknown diffusion coefficients, 2 Soret coefficients (and possibly one additional t_0). This approach was applied in [4] for ternary systems, but the authors chose to introduce strong simplifying assumption by neglecting the cross diffusion coefficients. The identification of the cross diffusion coefficients in ternary liquid systems is a very delicate step, as demonstrated by comparing the coefficients provided in [18,24] and [25].

For the method presented here, we selected reference images after the damping of the thermal transient, and have taken the advantage of the fact that species mass fractions evolve much slower than the thermal field. Images are analyzed in a region of interest excluding the liquid close to the copper blocks. Figure 5 shows that there is a good agreement between the fitting function $\text{d}\varphi_{i,\text{fit}}$ and the experimental data in the central region. The amplitude of the fitting error is larger in the region close to the lateral glass walls of the cell: over the thermodiffusive process, the concentration fields of the components align to the temperature field in the cell and show strong curvatures approaching the lateral walls. However, the fitting error is symmetrical with respect to the xz and yz central planes of the liquid volume. The $\sigma_{\Delta\varphi_i}$ are clearly influenced also by the duration of the runs: they are smaller than 1.2% for runs 18 and 23, and are reduced below 0.7% for the longer run (run 3). Those values were calculated for a fitting performed on a field of view including respectively 90% and 70% of the height and width of the cell. The main possible source of errors on the Soret coefficients arises from the accuracy on the measured contrast factors. However, in table 3, we provide the coefficients with two decimals to illustrate the reproducibility of the results obtained by processing several runs. The resulting maximal errors on the estimated Soret coefficients are smaller than 18% for all coefficients.

3.2 Measurement of diffusion coefficients

Two independent experiments were conducted in parallel, referred to as cell 1 and cell 2. The compositions of the liquid initially contained in the tubes, w_0, and of the liquid of the bath, w_∞, are reported in table 4. The overall composition of the experiment w_{exp} (set-point) is defined as the arithmetic mean of these two values.

For both cells, the initial solution in the tubes is more concentrated in THN, and is thus denser than the solution of the bath. The measured evolutions of the average compositions in the tubes for both experiments are reported in fig. 6.

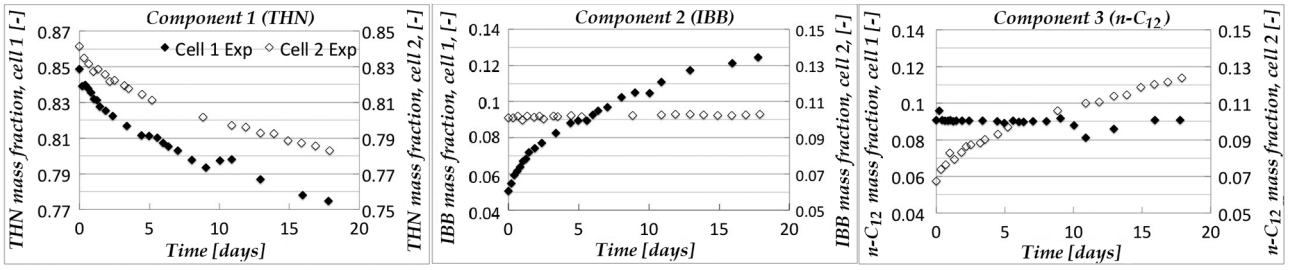

Fig. 6. Measured evolutions of the mass fractions of the three components obtained by ^{1}H NMR for the two independent OEC experiments.

Table 3. Soret separations an coefficients for the system THN-IBB-nC12 at $T = 25\,^\circ$C. Component 1 is 1,2,3,4-tetrahydronaphtalene, component 2 is isobutylbenzene and component 3 is n-dodecane.

Cell	Run	Δw_1	Δw_2	Δw_3	$S'_{T,1}$ ($10^{-3}\,\mathrm{K}^{-1}$)	$\Delta S'_{T,1}$ ($10^{-3}\,\mathrm{K}^{-1}$)	$S'_{T,2}$ ($10^{-3}\,\mathrm{K}^{-1}$)	$\Delta S'_{T,2}$ ($10^{-3}\,\mathrm{K}^{-1}$)	$S'_{T,3}$ ($10^{-3}\,\mathrm{K}^{-1}$)	$\Delta S'_{T,3}$ ($10^{-3}\,\mathrm{K}^{-1}$)
3	3	−0.0137	0.0086	0.0051	1.37	0.23	−0.86	0.14	−0.51	0.08
	18	−0.0136	0.0085	0.0051	1.36	0.24	−0.85	0.15	−0.51	0.09
	23	−0.0144	0.0098	0.0046	1.44	0.25	−0.98	0.17	−0.46	0.08
Mean value		−0.0139	0.0090	0.0049	1.39	0.24	−0.90	0.15	−0.49	0.08

Initial concentration differences between the liquids of the tubes and the bath are chosen very different for cells 1 and 2. Indeed, in cell 1, we applied initial concentration gradients for components 1 and 2 while the initial concentration gradient of component 3 is set to zero. Conversely, for cell 2, we applied initial concentration gradients for component 1 and 3 while the initial concentration gradient of component 2 is zero. In this way, in each cell, at time zero, we cancel selected terms in the diffusive fluxes. In other words, at the start of the experiment, we cancel selected terms in the coupled differential eqs. (4) and we try to isolate the different contributions in the diffusive fluxes. Of course, the diffusive couplings remain and it is impossible to cancel strictly their influence over time. In all the calculations performed, all the terms of eqs. (4) are considered. It is also observed in fig. 2 that the timeline of sampling is not linear over time. The time between two successive samples is shorter at the beginning of the experiments, about 6 hours. We gradually increase this time, so that after several days we collect one sample every 24 hours. We chose to operate in this manner because the concentration gradients are larger at short times, resulting in larger changes of the average concentration of the liquid of the tubes in the first days of experiment.

As expected, the evolutions of the concentrations of the different components follow typical multi-component diffusive profiles. However, the experimental profiles presented in fig. 2 include noise. In particular, for cell 1, for the measuring points between days 10 and 13, the mass fraction of component 1 is slightly higher than expected while the one of component 3 is slightly lower than expected. We attribute these effects to experimental errors whose origin is difficult to identify rigorously. In particular, the expected accuracy of the concentration measurement by NMR is very high and should not allow such experimental errors. There exist additional possible sources of errors in the OEC: the initial filling of the experimental cell is performed manually and it is always possible that unexpected convective mixing of the liquid modifies the initial concentration of the liquid of some tubes. The technique also requires opening the cell for sampling each tube. Finally limited evaporation is possible at the time of the sampling or when performing the dilution of the samples prior to the NMR measurements.

Table 4. Concentrations of the solutions for the two independent OEC experiments.

Cell	Component	w_0	w_∞	w_{exp}
1	1	0.8488	0.7500	0.7994
	2	0.0505	0.1500	0.1002
	3	0.1007	0.1000	0.1004
2	1	0.8414	0.7578	0.7996
	2	0.1012	0.1031	0.1021
	3	0.0574	0.1391	0.0983

Several interesting observations appear while studying the curves of fig. 6. First, the diffusion of component 1 is significantly different in both cells. This is mainly due to the different initial concentration differences between the liquids of the tubes and the bath for component 1 in the two cells, but also to the contributions of the diffusive couplings. Then, from our choice to cancel the concentrations differences of components 2 and 3 respectively for cells 1 and 2, we observe that the concentration evolutions do not

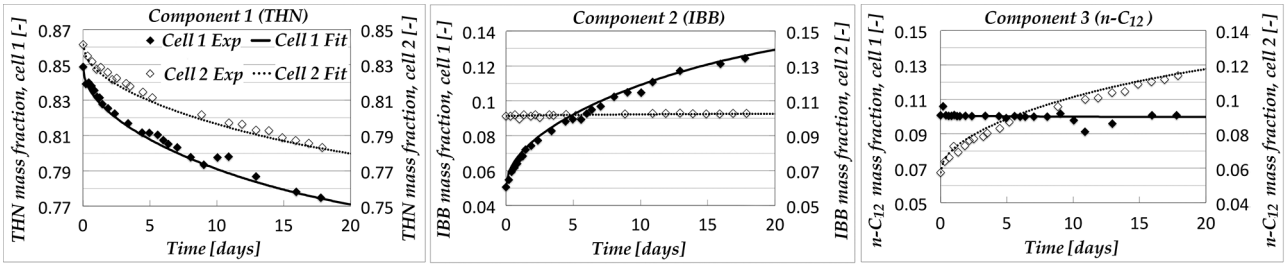

Fig. 7. Fitting of the evolutions of the mass fractions of the three components in both cells performed to obtain the matrix of molecular diffusion coefficients.

Table 5. Molecular diffusion coefficients and eigenvalues of the diffusion matrix for the system tetrahydronaphtalene, isobutylbenzene, dodecane, with mass fractions 0.8-0.1-0.1 at 25 °C measured by the Open Ended Capillary Technique.

D_{11} (10^{-10} m^2/s)	D_{12} (10^{-10} m^2/s)	D_{21} (10^{-10} m^2/s)	D_{22} (10^{-10} m^2/s)	$D^{\wedge 1}$ (10^{-10} m^2/s)	$D^{\wedge 2}$ (10^{-10} m^2/s)
5.5	−0.99	0.002	6.6	5.502	6.598
ΔD_{11} (10^{-10} m^2/s)	ΔD_{12} (10^{-10} m^2/s)	ΔD_{21} (10^{-10} m^2/s)	ΔD_{22} (10^{-10} m^2/s)	$\Delta D^{\wedge 1}$ (10^{-10} m^2/s)	$\Delta D^{\wedge 2}$ (10^{-10} m^2/s)
0.5	0.6	0.03	0.4	0.03	0.03

show the development of significant concentration gradients of those components at short times. This means that the diffusive couplings remain limited. This observation is not really surprising because the molecules involved in the studied system form a regular solution for which the association between the molecules are limited.

The measurement points collected for all samples for both cells are brought together to reconstruct the evolution of the average mass fractions of three components inside the tubes over time. The four diffusion coefficients are simultaneously estimated by fitting the 6 experimental curves of fig. 6 to the ternary diffusion equations.The fitting consists in minimizing the root mean square of the difference between the calculated and measured average concentration in the tubes, and detailed calculations were described in [26]. We used a Nelder and Mead simplex type algorithm for the optimization [27]. The minimization procedure is a delicate step: it appears that several regions of the parametric space provide local minimizers for the fitting function. This means that several very different diffusion matrices allow fitting the measurement points very satisfactorily. Additional physical constraints are added to the algorithm to avoid non-acceptable diffusion matrices. All the matrices that do not verify one of the following equations are rejected.

$$D_{11} + D_{22} > 0, \tag{11}$$

$$D_{11}D_{22} - D_{12}D_{21} > 0, \tag{12}$$

$$(D_{11} - D_{22})^2 + 4D_{12}D_{21} \geq 0. \tag{13}$$

These constraints are discussed in [28]. They appear naturally during the resolution of the multi-component diffusion equations and guarantee that the values of the principal diffusion coefficients are positive. Moreover, we introduced one additional condition for the minimization: we only consider diffusion matrices allowing fitting qualitatively simultaneously the 6 experimental curves of fig. 6. In other words, some matrices that provide lower values of the function f by approximating more accurately the evolution of 4 or 5 of the 6 curves, but resulting in a very different behaviour for the remaining component(s) are also rejected. This approach allows in particular avoiding diffusion matrices that would produce important concentration gradients of component 3 in cell 1 or component 2 in cell 2, that are not observed experimentally. Taking all this conditions into account, we obtain the diffusion matrices reported in table 5. In the table, we also provide the eigenvalues of the diffusion matrix, defined as [9]

$$D^{\wedge 1} = \frac{1}{2}\left(D_{11} + D_{22} - \sqrt{(D_{11} - D_{22})^2 + 4D_{12}D_{21}}\right), \tag{14}$$

$$D^{\wedge 2} = \frac{1}{2}\left(D_{11} + D_{22} + \sqrt{(D_{11} - D_{22})^2 + 4D_{12}D_{21}}\right). \tag{15}$$

The corresponding fitting curves are shown in fig. 7.

The fitting curves reproduce very reasonably the measured concentrations evolutions. However, performing the fitting simultaneously for both cells, the fitting curves do not pass exactly through the measured points. The errors ΔD_{ij} on each of the diffusion coefficients induced by the fitting procedure are estimated by computing the root mean square of the 6 experimental mass fractions curves divided by the derivative of the fitting function with re-

spect to each diffusion coefficients. As a result, it is important to note that the sensitivity of the proposed data processing technique on the cross diffusion coefficients D_{12} and D_{21} is low. The errors on the eigenvalues of the diffusion matrix $\Delta D^{\wedge i}$ are computed by evaluating the error propagation through eqs. (14) and (15).

4 Conclusions

The Soret coefficients of several compositions and temperatures of the THN-IBB-nC12 mixture were measured in the DSC cells of the DSC-DCMIX1 mission on board the International Space Station to provide reference data. This data is compared to different ground-based techniques in the frame of the benchmark described in [1]. We described the details of the data analysis for 3 runs and for the cell containing the 80-10-10 mixture at 25 °C.

Among the possible image processing methods and to obtain the phase fields from the flight data, it was selected here to i) obtain the phase fields by phase shifting algorithm, ii) to recalculate the random phase shifts that were obtained on SODI prior to the phase signals computations, iii) to use the Costantini algorithm for phase unwrapping.

Once the phase fields are obtained, they are fitted to a linear approximation, that corresponds to an ideal steady Soret separation. This fitting is discussed as function of the region of interest used. In particular, the region close to the center is the most insensitive to spatio-temporal unwanted nonlinearities. Also, we analyzed the validity of the linear approximation close the lateral transparent walls, where the profiles are clearly nonlinear. The relative error of the linear fitting in determining the actual phase fields can be made smaller than 0.8 percent by a good selection of the region of interest. By this direct analysis to obtain the Soret coefficients, we avoid the usage of uncertain diffusion coefficients. The analysis of the data shows also that stationarity approximation is satisfied.

We performed the measurement of the diffusion coefficients for the DCMIX1 benchmark system by the Open Ended Capillary technique. The measurements of the concentrations of the samples were obtained by ^{1}H NMR with a very high accuracy. We used an original experimental procedure that combines the experimental data collected through two independent experiments to evaluate the matrix of the diffusion coefficients. These two experiments differ by the initial concentration differences. For each of these experiments, the initial concentration of one of the three components is set to zero. This method is proposed to detect the couplings between the diffusive fluxes of the components. For the studied system, these couplings are not sufficiently strong to cause the development of significant concentration gradients for the component whose initial concentration gradient are set to zero. We report the entire matrix of diffusion coefficients as well as the eigenvalues of the diffusion matrix. Those values of the Soret and diffusion coefficients constitute our contribution to the DCMIX1 international experimental benchmark on molecular diffusion in ternary liquid system.

This work was supported by the SODiUM and DCMIX Prodex Programs funded by the Belgian federal Science Policy Office (SSTC). We are very grateful to the European Space Agency (ESA) for their constant support through this program. The Canadian Space Agency (CSA), the Russian Space Agency (Roscosmos) are also acknowledged for carrying the DCMIX on ISS, NASA for the access International Space Station, the members of the DCMIX Topical Team for valuable interest as well as C. Minetti and F. Dubois for their support for image processing.

References

1. M.M. Bou-Ali, A. Ahadi, D. Alonso de Mezquía, Q. Galand, M. Gebhardt, O. Khlybov, W. Köhler, M. Larrañaga, J.C. Legros, T. Lyubimova, A. Mialdun, I. Ryzhkov, M.Z. Saghir, V. Shevtsova, S. Van Varenbergh, "Benchmark values for the Soret, thermodiffusion and molecular diffusion coefficients of the ternary mixture tetralin+isobutylbenzene+n-dodecane with 0.8-0.1-0.1 mass fraction", this topical issue.
2. V. Shevtsova, T. Lyubimova, Z. Saghir, D. Melnikov, Y. Gaponenko, V. Sechenyh, J.C. Legros, A. Mialdun, J. Phys.: Conf. Ser. **327**, 012031 (2011) DOI: 10.1088/1742-6596/327/1/012031.
3. S.R. de Groot, P. Mazur, *Non-equilibrium thermodynamics* (Dover, New-York, 1984).
4. A. Ahadi, S. Van Vaerenbergh, M.Z. Saghir, J. Chem. Phys. **138**, 204201 (2013) DOI: 10.1063/1.4802984.
5. J.S. Anderson, K. Saddington, J. Chem. Soc. **2**, S381 (1975) DOI: 10.1039/JR949000S381.
6. J.N. Agar, V.M.M. Lobo, J. Chem. Soc. Faraday Trans. 1 **71**, 1659 (1975) DOI: 10.1039/F19757101659.
7. N.D. Kosov, I.V. Poyarkov, Meas. Techniques **37**, 581 (1994) DOI: 10.1007/BF00980450.
8. J.F. Dutrieux, J.K. Platten, G. Chavepeyer, M.M. Bou-Ali, J. Phys. Chem. B **106**, 6104 (2002) DOI: 10.1021/jp013945r.
9. A. Leahy-Dios, M.M. Bou Ali, J.K. Platten, A. Firoozabadi, J. Chem. Phys. **122**, 234502 (2005) DOI: 10.1063/1.1924503.
10. Q. Galand, M. Luhmer, S. Van Vaerenbergh, High Temp. High Pres. **38**, 329 (2010).
11. M. Larranaga, M. Bou-Ali, D. Soler, M. Martinez-Aguirre, A. Mialdun, M. Shevtsova, C. R. Mec. **341**, 356 (2013) DOI: 10.1016/j.crme.2013.01.008.
12. J.E. Greivenkamp, J.H. Bruning, "*Phase-shifting interferometry*," in *Optical Shop Testing*, edited by D. Malacara (Wiley, New York, 1992).
13. M. Takeda, H. Ina, J. Kobayashi, J. Opt. Soc. Am. **72**, 156 (1982).
14. T. Kreis, J. Opt. Soc. Am. **3**, 347 (1986) DOI: 10.1364/JOSAA.3.000847.
15. P. Hari Haran, B.F. Oreb, T. Eiju, Appl. Opt. **26**, 2504 (1987).
16. Zhaoyang Wang, Bongtae Han, Opt. Lett. **29**, 1671 (2004) DOI: 10.1364/OL.29.001671.
17. A. Mialdun, V. Shevtsova, J. Chem. Phys. **134**, 044524 (2011) DOI: 10.1063/1.3546036.
18. A. Mialdun, V. Shevtsova, C. R. Méc. **339**, 462 (2011) DOI: 10.1016/j.crme.2013.02.001.

19. D.J. Bone, Appl. Opt. **30**, 3627 (1991) DOI: 10.1364/AO.30.003627.
20. M. Costantini, IEEE Trans GARS **36**, 813 (1998) DOI: 10.1109/36.673674.
21. G. Wittko, W. Köhler, Philos. Mag. **83**, 2017 (2003).
22. S. Van Vaerenbergh, J.C. Legros, Phys. Rev. A **41**, 6727 (1990) DOI: 10.1103/PhysRevA.41.6727.
23. V.V. Sechenyh, J.C. Legros, V. Shevtsova, J. Chem. Thermodyn. **62**, 64 (2013) DOI: 10.1016/j.jct.2013.01.026.
24. A. Königer, H. Wunderlich, W. Köhler, J. Chem. Phys. **132**, 174506 (2010) DOI: 10.1063/1.3421547.
25. M. Larranaga, D. Andrew, M. Bou-Ali, J. Chem. Phys. **140**, 984503 (2014) DOI: 10.1063/1.4864189.
26. Q. Galand, S. Van Vaerenbergh, F. Montel, Energy Fuels **22**, 770 (2008) DOI: 10.1021/ef7004332.
27. M.J.D. Powel, Math. Prog. **4**, 193 (1973) DOI: 10.1007/BF01584660.
28. R. Taylor, R. Krishna, *Multicomponent Mass Transfer* (Wiley, New York, 1976).